Semi-Blind Image Restoration Via Mumford–Shah Regularization

Leah Bar, Nir Sochen, and Nahum Kiryati, *Senior Member, IEEE*

***Abstract*—Image restoration and segmentation are both classical problems, that are known to be difficult and have attracted major research efforts. This paper shows that the two problems are tightly coupled and can be successfully solved together. Mutual support of image restoration and segmentation processes within a joint variational framework is theoretically motivated, and validated by successful experimental results. The proposed variational method integrates semi-blind image deconvolution (parametric blur-kernel), and Mumford–Shah segmentation. The functional is formulated using the Γ-convergence approximation and is iteratively optimized via the alternate minimization method. While the major novelty of this work is in the unified treatment of the semi-blind restoration and segmentation problems, the important special case of known blur is also considered and promising results are obtained.**

***Index Terms*—Blind deconvolution, Mumford–Shah segmentation, variational image restoration.**

I. Introduction

IMAGE analysis systems usually operate on blurred and noisy images. The standard model $g = h * f + n$ is applicable to a large variety of image degradation processes that are encountered in practice. Here h represents an (often unknown) space-invariant blur kernel (point spread function), n is the noise and f is an ideal version of the observed image g.

The two following problems are at the basis of successful image analysis: 1) Can we estimate the blur kernel h and recover f? and 2) Can we segment g in agreement with the structure of f? Blind restoration and image segmentation are both classical problems, that are known to be difficult and have attracted major research efforts, see, e.g., [3], [12], [13], and [20].

Had the correct segmentation of the image been known, blind image restoration would have been facilitated. Clearly, the blur kernel could have then been estimated based on the smoothed profiles of the known edges. Furthermore, denoising could have been applied to the segments without over-smoothing the edges. Conversely, had adequate blind image restoration been accomplished, successful segmentation would have been much easier to achieve. Blind restoration and image segmentation are therefore tightly coupled tasks: the solution of either problem would become fairly straightforward given that of the other.

This paper presents an integrated framework for simultaneous semi-blind restoration and image segmentation. As will be seen, strong arguments exist in favor of constraining the recovered blur kernel to parameterized function classes, see e.g., [6]. Our approach is presented in the context of the fundamentally important model of isotropic Gaussian blur, parameterized by its (unknown) width. Preliminary results were presented in [4].

II. Fundamentals

A. Segmentation

The difficulty of image segmentation is well known. Successful segmentation requires top-down flow of models, concepts and *a priori* knowledge in addition to the image data itself. In their segmentation method, Mumford and Shah [14] introduced top-down information via the preference for piecewise-smooth segments separated by well-behaved contours. Formally, they proposed to minimize a functional that includes a fidelity term, a piecewise-smoothness term, and an edge integration term

$$\mathcal{F}(f,K) = \frac{1}{2}\int_{\Omega}(f-g)^2 dA + \beta\int_{\Omega\setminus K}|\nabla f|^2 dA + \alpha\int_{K} d\sigma. \tag{1}$$

Here, K denotes the edge set and $\int_K d\sigma$ is the total edge length. The coefficients α and β are positive regularization constants. The primary difficulty in the minimization process is the presence of the unknown discontinuity set K in the integration domains.

The Γ-convergence framework approximates an irregular functional $\mathcal{F}(f,K)$ by a sequence $\mathcal{F}_\epsilon(f)$ of regular functionals such that

$$\lim_{\epsilon\to 0}\mathcal{F}_\epsilon(f) = \mathcal{F}(f,K)$$

and the minimizers of $\mathcal{F}_\epsilon$ approximate the minimizer of $\mathcal{F}$. Ambrosio and Tortorelli [1] applied this approximation to the Mumford–Shah functional, and represented the edge set by a characteristic function $(1-\chi_K)$ which is approximated by an auxiliary function v, i.e., $v(x)\approx 0$ if $x\in K$ and $v(x)\approx 1$ otherwise. The functional thus takes the form

$$\mathcal{F}_\epsilon(f,v) = \frac{1}{2}\int_{\Omega}(f-g)^2 dA + \beta\int_{\Omega} v^2|\nabla f|^2 dA + \alpha\int_{\Omega}\left(\epsilon|\nabla v|^2 + \frac{1}{4\epsilon}(v-1)^2\right) dA. \tag{2}$$

Manuscript received July 25, 2004; revised March 3, 2005. The work of L. Bar was supported by the Weinstein Center for Signal Processing Research, Tel-Aviv University. This work was supported by MUSCLE: Multimedia Understanding through Semantics, Computation and Learning, a European Network of Excellence funded by the EC 6th Framework IST Programme, and also by the Israel Academy of Sciences. The associate editor coordinating the review of this manuscript and approving it for publication was Dr. Mario A. T. Figueiredo.

L. Bar and N. Kiryati are with the School of Electrical Engineering, Tel Aviv University, Tel Aviv 69978, Israel (e-mail: nk@eng.tau.ac.il).

N. Sochen is with the Department of Applied Mathematics, Tel Aviv University, Tel Aviv 69978, Israel.

Digital Object Identifier 10.1109/TIP.2005.863120

(See also Richardson and Mitter [16].) Discretization of the Mumford–Shah functional and its Γ-convergence approximation is considered in [7]. Additional perspectives on variational segmentation can be found in Vese and Chan [23] and in Samson *et al.* [19].

Simultaneous segmentation and restoration of a blurred and noisy image has recently been presented in [11]. A variant of the Mumford–Shah functional was approached from a curve evolution perspective. In that work, the discontinuity set is limited to an isolated closed curve in the image and the blurring kernel h is assumed to be *a priori* known.

B. Restoration

Restoration of a blurred and noisy image is difficult even if the blur kernel h is known. Formally, finding f that minimizes

$$||h * f - g||^2_{L_2(\Omega)} \tag{3}$$

is an ill-posed inverse problem: small perturbations in the data may produce unbounded variations in the solution. In Tikhonov regularization [22], a smoothing term $\int_\Omega |\nabla f|^2 dA$ is added to the fidelity functional (3). In image restoration, Tikhonov regularization leads to over-smoothing and loss of important edge information. For better edge preservation, the Total Variation approach [17], [18] replaces L_2 smoothing by L_1 smoothing. The functional to be minimized is thus

$$\mathcal{F}(f,h) = \frac{1}{2}||h * f - g||^2_{L_2(\Omega)} + \beta \int_\Omega |\nabla f| dA. \tag{4}$$

This nonlinear optimization problem can be approached via the half-quadratic minimization technique [2], [9], [10]. An efficient alternative approach, based on the lagged diffusivity fixed point scheme and conjugate gradients iterations, was suggested by Vogel and Oman [24].

Image restoration becomes even more difficult if the blur kernel h is not known in advance. In addition to being ill-posed with respect to the image, the blind restoration problem is ill-posed in the kernel as well. To illustrate one aspect of this additional ambiguity, suppose that h represents isotropic Gaussian blur, with variance $\sigma^2 = 2t$

$$h_t = \frac{1}{4\pi t} e^{-\frac{x^2+y^2}{4t}}.$$

The convolution of two Gaussian kernels is a Gaussian kernel, the variance of which is the sum of the two originating variances

$$h_{t_1} * h_{t_2} = h_{t_1+t_2}. \tag{5}$$

Assume that the true t of the blur kernel is $t = T$, so $g = h_T * f$. The fidelity term (3) is obviously minimized by f and h_T. However, according to (5), g can also be expressed as

$$g = h_{t_1} * h_{t_2} * f \quad \forall (t_1 + t_2) = T.$$

Therefore, an alternative hypothesis, that the original image was $h_{t_2} * f$ and the blur kernel was h_{t_1}, minimizes the fidelity term just as well. This exemplifies a fundamental ambiguity in the division of the apparent blur between the recovered image and the blur kernel, i.e., that the scene itself might be blurred. For meaningful image restoration, this hypothesis must be rejected and the largest possible blur should be associated with the blur kernel. It can be achieved by adding a kernel-smoothness term to the functional.

Blind image restoration with joint recovery of the image and the kernel, and regularization of both, was presented by You and Kaveh [26], followed by Chan and Wong [8]. Chan and Wong suggested to minimize a functional consisting of a fidelity term and total variation (L_1 norm) regularization for both the image and the kernel

$$\mathcal{F}(f,h) = \frac{1}{2}||h * f - g||^2_{L_2(\Omega)} + \alpha_1 \int_\Omega |\nabla f| dA + \alpha_2 \int_\Omega |\nabla h| dA. \tag{6}$$

In their iterative algorithm, the recovered image f is initialized as the observed image g, and the blur kernel h as the impulse function. The parameters α_1 and α_2 control the L_1-smoothness of the recovered image and the kernel respectively. As α_1 is increased, the recovered image becomes smoother, at the expense of lower fidelity and a narrow kernel. Increasing the parameter α_2 would lead to a wider kernel, at the expense of lower fidelity and ringing in the recovered image. Much can be learned about the blind image restoration problem by studying the characteristics and performance of this algorithm. Consider the images shown in Fig. 1. An original image (upper left) is degraded by isotropic Gaussian blur with $\sigma = 2.1$ (top-right). Applying the algorithm of [8] (with $\alpha_1 = 10^{-4}$ and $\alpha_2 = 10^{-4}$) yields a recovered image (bottom-left) and an estimated kernel (bottom-right). It can be seen that the identification of the kernel is inadequate, and that the image restoration is sensitive to the kernel recovery error.

To obtain deeper understanding of these phenomena, we plugged the original image f and the degraded image g into the functional (6), and carried out minimization only with respect to h. The outcome was similar to the kernel shown in Fig. 1 (bottom-right). This demonstrates an excessive dependence of the recovered kernel on the image characteristics. At the source of this problem is the aspiration for general kernel recovery: the algorithm of [8] imposes only mild constraints on the shape of the reconstructed kernel. This allows the distribution of edge directions in the image to have an influence on the shape of the recovered kernel, via the trade-off between the fidelity and kernel smoothness terms. In the example of Fig. 1, there are more vertical edges than horizontal ones. Since the functional (6) trades between the smoothness of the estimated kernel and the smoothness of the recovered image, it has an incentive to overestimate the vertical scale of the kernel. That is because the resulting penalty in image smoothness (ringing across the few horizontal edges) is relatively small. For additional insight, see Fig. 2.

Facing the ill-posedness of blind restoration with a general kernel, two approaches can be taken. One is to add relevant data; the other is to constrain the solution. Recent studies have adopted one of these two approaches, or both. In [21], the blind restoration problem is considered within a multichannel framework, where *several* input images can be available.

In many practical situations, the blurring kernel can be modeled by the physics/optics of the imaging device and the set-up.

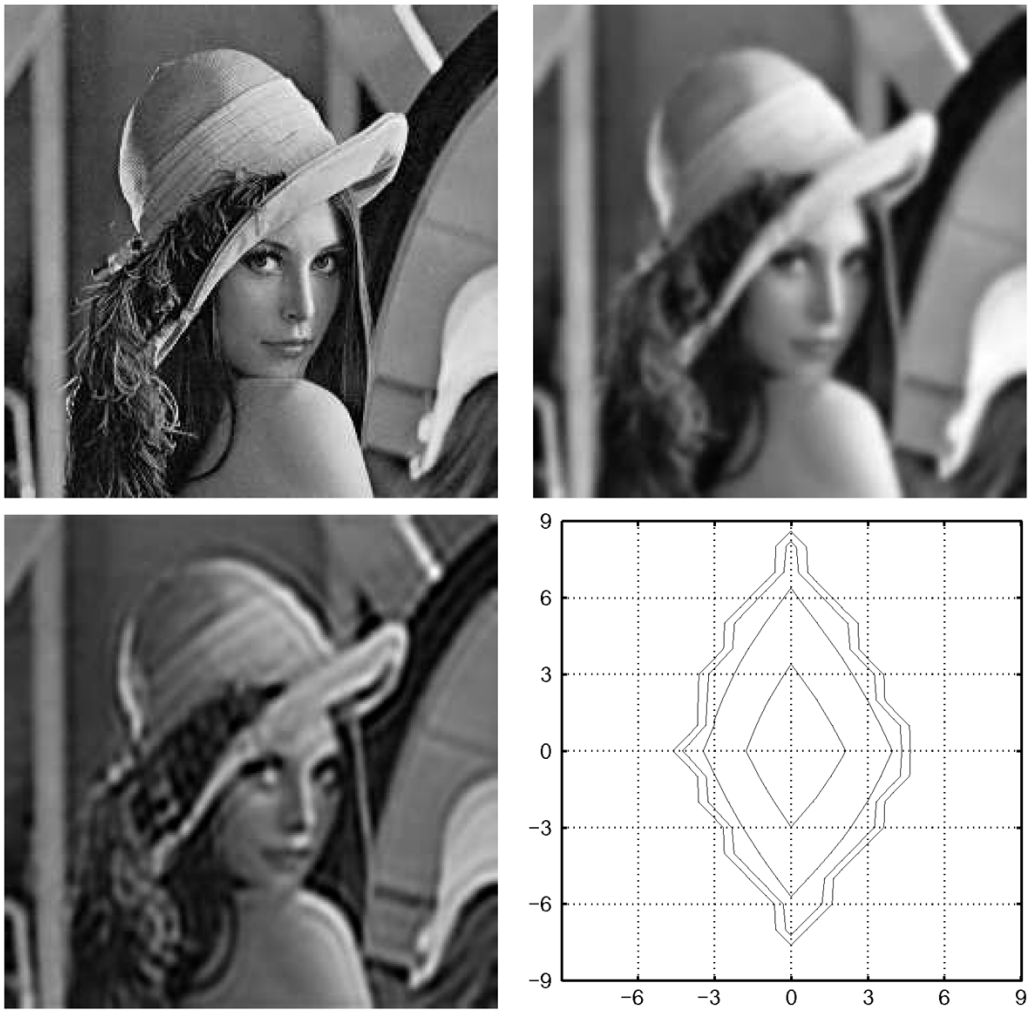

Fig. 1. Blind image restoration using the method of [8]. Top left: Original. Top right: Blurred using an isotropic Gaussian kernel ($\sigma = 2.1$). Bottom left: Recovered image. Bottom right: Reconstructed kernel.

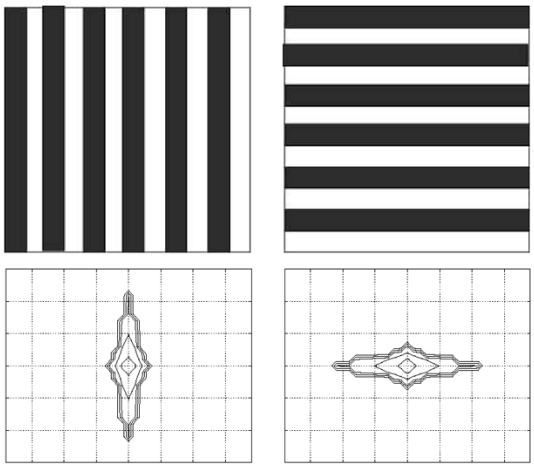

Fig. 2. Experimental demonstration of the dependence of the recovered kernel on the image characteristics in [8]. Each of the two synthetic bar images (top-row) was smoothed using an isotropic Gaussian kernel, and forwarded to the blind restoration algorithm of [8] (6). The respective recovered kernels are shown in the bottom row.

The blurring kernel can then be constrained and described as a member in a class of parametric functions. This constraint was exploited in the direct blind deconvolution algorithm of [6]. In [15], additional relevant data was introduced via learning of similar images and the blur kernel was assumed to be Gaussian.

By modifying the framework of [8], we can demonstrate the gains that can be obtained by reducing the blind image restoration problem to semi-blind restoration, in which the kernel is assumed to belong to a class of parametric functions. Fig. 3 is obtained by forcing the algorithm to restrict the estimated kernel to isotropic Gaussians of unknown width. The parameters in this example were $\alpha_1 = 10^{-4}$ and $\alpha_2 = 2$, and the estimated σ was 1.94. The significant improvement with respect to Fig. 1 (bottom left) is clear.

III. Coupling Semi-Blind Restoration With Segmentation

The observation, discussed in the introduction, that blind restoration and image segmentation can be mutually supporting, is the fundamental motivation for this work. We present an algorithm, based on functional minimization, that iteratively alternates between segmentation, parametric blur identification and restoration. We note that large classes of practical imaging problems are compatible with constrained blur models. In particular, Carasso [6] described the association of the Gaussian

Fig. 3. Semi-blind restoration obtained by restricting the algorithm of [8] to isotropic Gaussian kernels of unknown width. Compare with Fig. 1 (bottom-left).

case with diverse applications such as undersea imaging, nuclear medicine, computed tomography scanners, and ultrasonic imaging in nondestructive testing.

In this work, we integrate Mumford–Shah segmentation with semi-blind deconvolution of isotropic Gaussian blur. This is accomplished by extending the Mumford–Shah functional and applying the Γ-convergence approximation as described in [1]. The observed image g is modeled as $g = h_\sigma * f + n$ where h_σ is an isotropic Gaussian kernel parameterized by its width σ, and n is white Gaussian noise. The objective functional used is

$$\mathcal{F}_\epsilon(f, v, \sigma) = \frac{1}{2}\int_\Omega (h_\sigma * f - g)^2 dA + G_\epsilon(f, v) + \gamma \int_\Omega |\nabla h_\sigma|^2 dA \quad (7)$$

where $G_\epsilon(f, v)$ is the image regularization term, defined as

$$G_\epsilon(f, v) = \beta \int_\Omega v^2 |\nabla f|^2 dA + \alpha \int_\Omega \left(\epsilon |\nabla v|^2 + \frac{(v-1)^2}{4\epsilon}\right) dA.$$

In the sequel, it is assumed that the image domain Ω is a rectangle in $\mathbb{R}^2$ and that image intensities are normalized to the range $[0, 1]$.

The functional depends on the functions f (ideal image) and v (edge integration map), and on the width parameter σ of the blur kernel h_σ. The fidelity term accounts for the blur process $h_\sigma * f$. Braides [5] presents a proof for the Γ-convergence of G_ϵ to the regularization terms in the Mumford–Shah functional (1).

The last term in (7) stands for the regularization of the kernel, necessary to resolve the fundamental ambiguity in the division of the apparent blur between the recovered image and the blur kernel. This means that we prefer to reject the hypothesis that the blur originates from f, and assume that it is due to the convolution with the blur kernel. From the range of possible kernels, we thus select a wide one. This preference is represented by the kernel smoothness term: the width of the Gaussian corresponds to its smoothness, measured by the L_2 norm of its gradient. The convenient L_2 norm was preferred because the blur kernels are restricted to Gaussians, that are smooth functions. Note that the kernel regularization term in [8] had to use the L_1 norm, because they admitted piecewise smooth kernels.

Minimization of the objective functional (7) with respect to f and v is carried out using the Euler-Lagrange (E-L) equations (8) and (9), with Neumann boundary conditions. The E-L equations are *linear* partial differential equations; their derivation is presented in Appendix A. Minimization with respect to the scalar parameter σ is determined by differentiation of the objective functional (10)

$$\frac{\delta \mathcal{F}_\epsilon}{\delta v} = 2\beta v |\nabla f|^2 + \alpha \cdot \frac{v-1}{2\epsilon} - 2\epsilon\alpha \nabla^2 v = 0 \quad (8)$$

$$\frac{\delta \mathcal{F}_\epsilon}{\delta f} = (h_\sigma * f - g) * h_\sigma(-x, -y) - 2\beta \mathrm{Div}(v^2 \nabla f) = 0 \quad (9)$$

$$\frac{\partial \mathcal{F}_\epsilon}{\partial \sigma} = \int_\Omega \left[(h_\sigma * f - g)\left(\frac{\partial h_\sigma}{\partial \sigma} * f\right) + \gamma \frac{\partial}{\partial \sigma}|\nabla h_\sigma|^2\right] dA = 0 \quad (10)$$

where in (10)

$$\frac{\partial h_\sigma}{\partial \sigma} = \frac{1}{2\pi\sigma^2} e^{-\frac{x^2+y^2}{2\sigma^2}} \cdot \left(\frac{x^2+y^2}{\sigma^3} - \frac{2}{\sigma}\right) \quad (11)$$

and

$$\frac{\partial}{\partial \sigma}|\nabla h_\sigma|^2 = \frac{1}{2\pi^2\sigma^4} e^{-\frac{x^2+y^2}{\sigma^2}} \cdot \left(\frac{x^2+y^2}{\sigma^7} - \frac{4}{\sigma^5}\right). \quad (12)$$

Studying the objective functional (7), it can be seen that it is strictly convex and lower bounded with respect to the functions f and v if the other one and the blur kernel h_σ are fixed. The convexity property also holds for general blur kernels $h(x, y)$. However, because of the nonlinear dependence of h_σ on σ, the functional is not convex with respect to σ. Nevertheless, no convergence problems have been encountered in our experiments. Note that since the Gaussian is an even function, the search for σ can be limited to positive values. Following [8], the alternate minimization (AM) approach is applied: in each step of the iterative procedure we minimize with respect to one function and keep the other two fixed. This leads to a local minimum. The following algorithm is obtained:

`Initialization`: $f = g, \sigma = \varepsilon_1, v = 1, \sigma_{\mathrm{prev}} \gg 1$

`while`$(|\sigma_{\mathrm{prev}} - \sigma| > \varepsilon_2)$ repeat

1. Solve (8) for v.
2. Solve (9) for f.
3. Set $\sigma_{\mathrm{prev}} = \sigma$, and solve (10) for σ.

Here ε_1 and ε_2 are small positive constants.

IV. Discrete Solution

The essence of the proposed algorithm is iterative solution of the linear partial differential equation (8), (9), and (10). These equations are discretized and solved numerically.

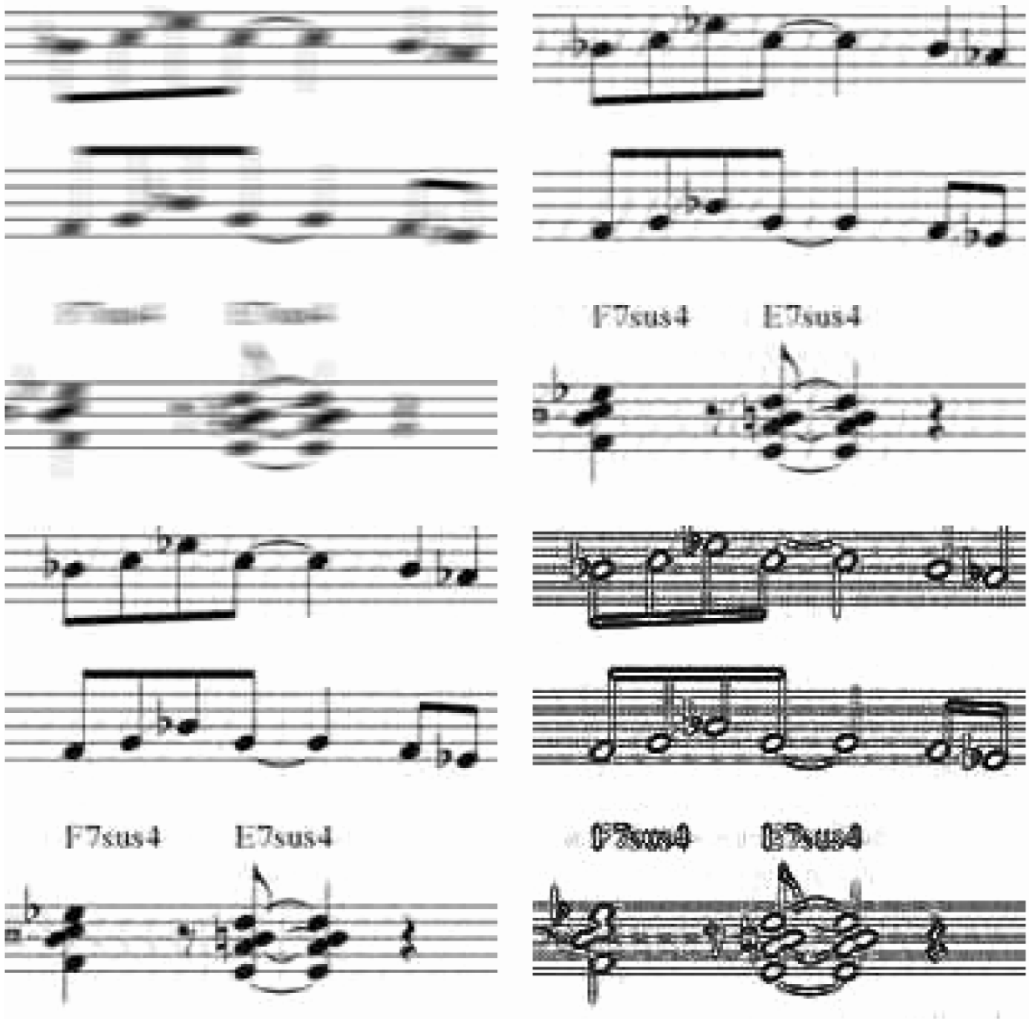

Fig. 4. Case of a known (9-pixel horizontal motion) blur kernel. Top left: Corrupted image. Top right: Restoration using the TV method [17], [24]. Bottom left: Restoration using the suggested method. Bottom right: Edge map produced by the suggested method.

The discretization scheme used was cell-centered finite difference (CCFD) [21], [24]. Consider a function $u(x,y)$ defined above the unit square. In CCFD, the domain is divided into $M \times M$ identical $h \times h$ cells ($h = 1/M$), and $u(x,y)$ is approximated by a function $U(x,y)$ that is constant within each cell. Formally, the cell centers are (x_i, y_j), where

$$x_i = (i - 1/2)h, \quad i = 1, \ldots, M \tag{13}$$

$$y_j = (j - 1/2)h, \quad j = 1, \ldots, M \tag{14}$$

and $U(x_i, y_j) = u(x_i, y_j)$. The forward and backward finite difference approximations of the derivatives $\partial u(x,y)/\partial x$ and $\partial u(x,y)/\partial y$ are respectively denoted by $\Delta^x_{\pm} u_{ij} = \pm(u_{i\pm1,j} - u_{ij})$ and $\Delta^y_{\pm} u_{ij} = \pm(u_{i,j\pm1} - u_{ij})$.

Step 1 of the algorithm calls for the solution of (8). Following discretization, we obtain a linear system of equations

$$2\beta v_{ij}[(\Delta^x_+ f_{ij})^2 + (\Delta^y_+ f_{ij})^2] + \alpha \cdot \frac{v_{ij} - 1}{2\epsilon} - 2\alpha\epsilon(\Delta^x_- \Delta^x_+ v_{ij} + \Delta^y_- \Delta^y_+ v_{ij}) = 0. \tag{15}$$

With column-stack ordering of $\{v_{ij}\}$, this system is of the form $Pv = q$, where the matrix P is symmetric and sparse. It is solved using the Minimal Residual algorithm [25].

Let H_σ denote the operator of convolution with a Gaussian h_σ, i.e., $H_\sigma f = h_\sigma(x,y) * f$. H^*_σ is the adjoint operator, $H^*_\sigma f = h_\sigma(-x,-y) * f$. Using the notation of [24], let $L(v)$ denote the differential operator

$$L(v)f = -\mathrm{Div}(v^2 \nabla f). \tag{16}$$

Now, (9) can be expressed as

$$H^*_\sigma(H_\sigma f - g) + 2\beta L(v) f = 0 \tag{17}$$

Let $A(v)f = H_\sigma H^*_\sigma f + 2\beta L(v) f$. Rearranging (17), we obtain

$$A(v)f = H^*_\sigma g \tag{18}$$

f is iteratively determined. To obtain f^{n+1}, a correction term d^n is added to the current value f^n : $f^{n+1} = f^n + d^n$. d^n is estimated by

$$A(v)d^n = H^*_\sigma g - A(v)f^n. \tag{19}$$

In Appendix B, it is shown that the operator $A(v)$ is self-adjoint and positive definite. In the discrete domain, (19) corresponds to a linear system of equations with a symmetric and positive

Fig. 5. Semi-blind restoration. Top left: Blurred ($\sigma = 2.1$) image. Top right: Restoration using the method of [8]. Bottom left: Restoration using a modified version of [8], in which the kernel was restricted to the family of isotropic Gaussians. Bottom right: Restoration using the method suggested in this paper.

definite matrix $A(v)$. Consequently, (19) is solved for d^n via the Conjugate Gradients method. In step 3, (10) takes the form

$$\sum_{i,j\in\Omega}(h_\sigma * f - g)\left(\frac{\partial h_\sigma}{\partial\sigma} * f\right)_{i,j} + \gamma \sum_{i,j\in\Omega}\left(\frac{\partial}{\partial\sigma}|\nabla h_\sigma|^2\right)_{i,j} = 0 \tag{20}$$

where $\partial h_\sigma/\partial\sigma$ and $\partial(|\nabla h_\sigma|^2)/\partial\sigma$ are given in (11) and (12), respectively. The equation was solved for σ using the bisection method. The discrete support of the Gaussian was limited to about $20\sigma \times 20\sigma$, which in our experiments was much smaller than the image size. The numerical integral of h_σ was normalized to 1.

V. Special Case: Known Blur Kernel

If the blur kernel is known, the restriction to Gaussian kernels is no longer necessary. In this case, the kernel-regularization term in the objective functional (7) can be omitted. Consequently, the algorithm can be simplified by skipping step 3 and replacing the stopping criterion by a simple convergence measure.

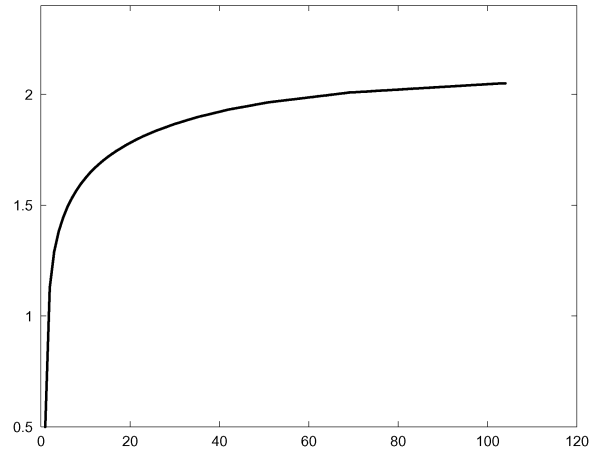

Fig. 6. Convergence of the estimated width σ of the blur kernel as a function of the iteration number in the semi-blind recovery of the *noiseless coin* image (Fig. 5).

The resulting algorithm for coupled segmentation and image restoration is fast, robust and stable. Unlike [11], the discontinuity set is not restricted to isolated closed contours. Its performance is exemplified in Fig. 4. The top-left image in Fig. 4 is a blurred version of an original 170×170 *Notes* image (not

Fig. 7. Semi-blind restoration with some additive noise ($\mathrm{SNR} = 30$ dB). Top left: Blurred ($\sigma = 2.1$) and noisy image. Top right: Restoration using the method of [8]. Bottom left: Restoration using the modified version of [8], in which the kernel was restricted to the family of isotropic Gaussians. Bottom right: Restoration using the suggested method.

shown). The blur kernel corresponds to horizontal 9-pixel motion. The top-right image is the reconstruction obtained using total variation regularization [17], [24], with a regularization parameter of $3 \cdot 10^{-7}$. The bottom-left image is the outcome of the proposed method ($\beta = 10^{-4}, \alpha = 10^{-8}, \epsilon = 10^{-3}$), with a known blur kernel. The bottom-right image shows the associated edge map v determined by the algorithm. Acceptable restoration is obtained with both methods. Nevertheless, the suggested method yields a sharper result, and is almost free of "ghosts" (white replications of notes) that can be seen in the top-right image (e.g., between the C notes in the right part of the top stave). Computing time was about 2 min in interpreted MATLAB on a 2-GHz PC.

VI. Results: Semi-Blind Restoration

Consider the example shown in Fig. 5. The top-left image was obtained by blurring the original 200×200 *coin* image (not shown) with a Gaussian kernel with $\sigma = 2.1$. Restoration using [8] ($\alpha_1 = 10^{-4}, \alpha_2 = 10^{-5}$) is shown top-right. The bottom-left image is the outcome of a modified version of the method of [8]. The kernel was restricted to the family of isotropic Gaussians, and kernel smoothness was measured using the L_2 norm. The parameters were tuned for best performance: $\alpha_1 = 10^{-4}$ and $\alpha_2 = 20$. The resulting estimate of σ was 1.61. The gains brought by the restriction of the recovered kernel to a class of parametric kernels are clear. The image recovered using the method suggested in this paper shown bottom-right. In this case the parameters were $\beta = 10^{-4}, \alpha = 10^{-8}, \epsilon = 10^{-3}, \gamma = 20$ and the resulting estimate of σ was 2.05. Note that the bottom-right image, corresponding to our method, is sharper than the bottom-left image. This highlights the advantage of the Mumford–Shah image regularizer over the L_1 norm. The convergence process is illustrated in Fig. 6.

In Fig. 7, the blurred input image (top-left) is similar to that of Fig. 5, but with slight white Gaussian noise added ($\mathrm{SNR} = 30$ dB). Shown top-right is the image recovered using the method of [8] ($\alpha_1 = 10^{-4}, \alpha_2 = 10^{-4}$). The bottom-left image is the outcome of the modified version of the method of [8]. The kernel was restricted to the family of isotropic Gaussians and kernel smoothness was measured using the L_2 norm. Here $\alpha_1 = 0.01, \alpha_2 = 60$ and the resulting estimate of σ was 1.33. The gains brought by the restriction of the recovered

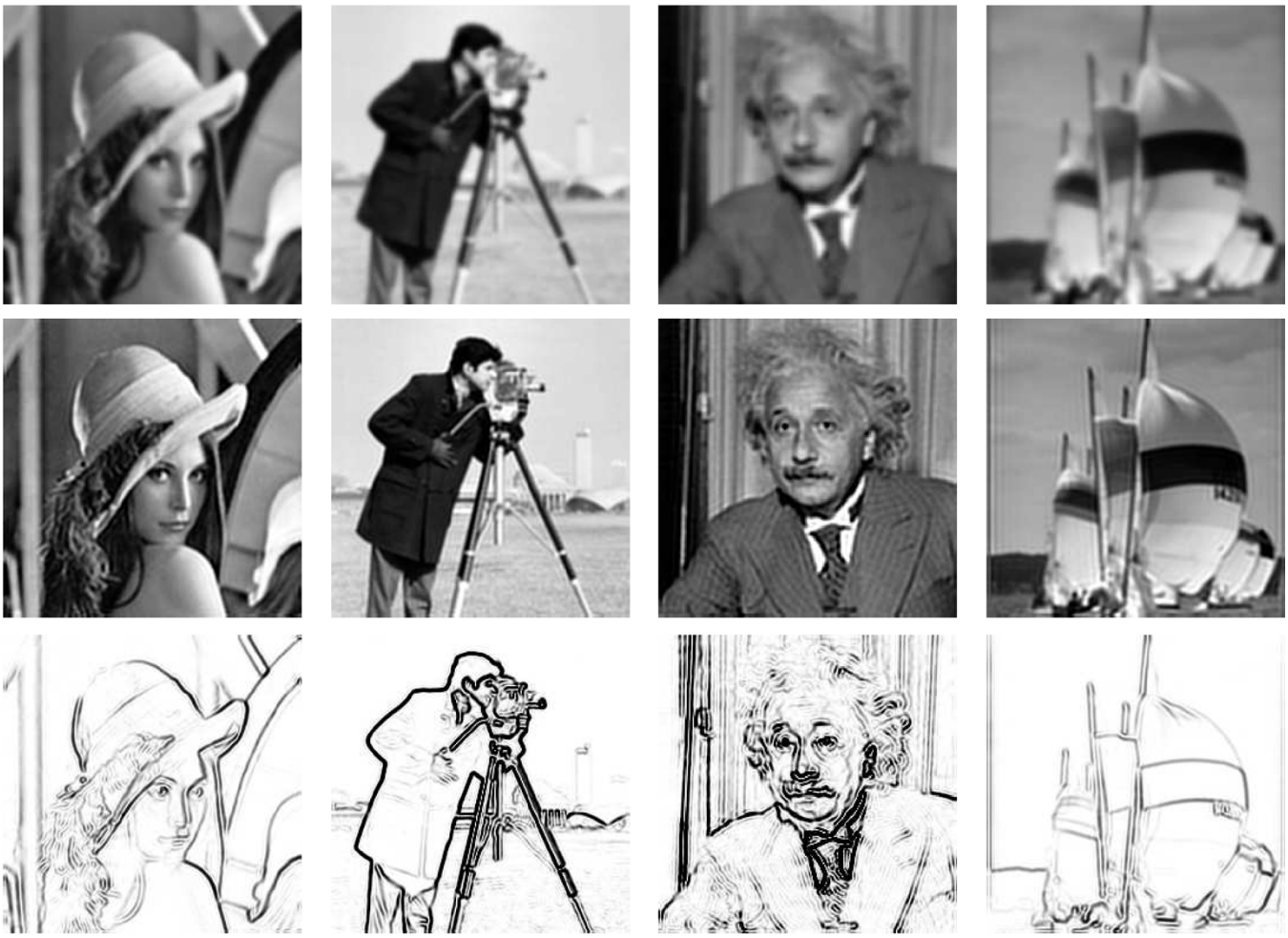

Fig. 8. Semi-blind restoration. Top row: Blurred images. Middle row: Restoration using the suggested method. Bottom row: Edge maps produced by the suggested method.

kernel to a class of parametric kernels are again clear. The image recovered using the method suggested in this paper is shown bottom-right ($\beta = 0.01, \alpha = 0.001, \epsilon = 0.1, \gamma = 60$). The resulting estimate of σ was 1.77.

Note that in the presence of noise, the image and kernel smoothness parameters are increased in order to compensate for the noise, and the resulting σ is decreased. Nevertheless, with or without noise, and even though $\gamma = \alpha_2$, the suggested method yields better (higher) estimates of σ, and consequently sharper recovered images.

In all the experiments described in the sequel, the parameters used in the algorithm were $\beta = 10^{-4}, \alpha = 10^{-8}, \epsilon = 10^{-3}$, and $\gamma = 40$. The initial value of σ was 0.5 and the convergence tolerance was $\varepsilon_2 = 10^{-2}$.

Additional examples are shown in Fig. 8. The top, middle and bottom rows correspond to the blurred, recovered and edge images respectively. The images were blurred using a Gaussian kernel with $\sigma = 2.1$ for the *Lena*, *Cameraman* and *Einstein* images, and $\sigma = 2.6$ for the *Sails* image. Computing time in these examples was about 12 minutes in interpreted MATLAB on a 2 GHz PC. The unknown width parameters of the blur kernels were estimated to be $\sigma = 2.01, 1.95, 2.27, 2.57$, and are in pleasing agreement with their true value.

VII. Discussion

Inverse problems in image analysis are difficult and often ill-posed. This means that searching for the solution in the largest possible space is not always the best strategy. *A priori* knowledge should be used, wherever possible, to limit the search and constrain the solution. In the context of pure blind restoration, Carasso [6] analyzes previous approaches and presents convincing arguments in favor of restricting the class of blurs.

Along these lines, in this paper the blur kernels are constrained to the class of isotropic Gaussians parameterized by their width. This is a sound approximation of physical kernels encountered in diverse contexts [6]. The advantages brought by this restriction are well-demonstrated in the experimental results that we provide.

In the suggested variational framework, the restored image is regularized using the Mumford–Shah terms ($G_\epsilon(f, v)$). This is a better model than the L_1 norm for the piecewise smoothness of

common images, and leads to better experimental results. The experimental results also demonstrate the robustness of the algorithm with respect to the parameters. The images tested in Fig. 8 are quite different, yet they were all successfully restored using the same parameter set.

The functional (7) is not generally convex. Nevertheless, the algorithm gracefully converged to a visually appealing restoration in all our experiments. The risk of convergence to local minima is common and inherent to most variational image processing algorithms. Only in special cases can convergence to the global minimum be proved. This is an interesting and challenging topic for future research.

APPENDIX A

In this Appendix we derive the Euler-Lagrange equations (8) and (9) that correspond to the objective functional (7)

$$\mathcal{F}_\epsilon(f,v,\sigma)=\frac{1}{2}\int_\Omega (h_\sigma * f-g)^2 dA+\beta\int_\Omega v^2|\nabla f|^2 dA +\alpha\int_\Omega\left(\epsilon|\nabla v|^2+\frac{(v-1)^2}{4\epsilon}\right)dA+\gamma\int_\Omega|\nabla h_\sigma|^2 dA.$$

In the following derivation, let $f(x,y)$ be extended to the whole $\mathbb{R}^2$ with the Neumann boundary condition, meaning that the function values are uniform along the normal of the image boundary. In addition, the integration element dA denotes $dxdy$.

1) Variation With Respect to f: The variation of $\mathcal{F}_\epsilon$ with respect to f can be expressed as

$$\frac{\delta\mathcal{F}_\epsilon}{\delta f}=\frac{\partial}{\partial\lambda}\mathcal{F}_\epsilon(f+\lambda\eta)\bigg|_{\lambda=0}=\frac{\partial}{\partial\lambda}\left[\mathcal{F}_\epsilon^I+\mathcal{F}_\epsilon^{II}\right]\bigg|_{\lambda=0}=0$$

where $\eta\in C^1(\Omega)$ with

$$\mathcal{F}_\epsilon^I=\frac{1}{2}\int_\Omega[h_\sigma*(f+\lambda\eta)-g]^2 dA$$

and

$$\mathcal{F}_\epsilon^{II}=\beta\int_\Omega v^2[(f_x+\lambda\eta_x)^2+(f_y+\lambda\eta_y)^2]dA.$$

For the first part

$$\frac{\partial\mathcal{F}_\epsilon^I}{\partial\lambda}\bigg|_{\lambda=0}=\int_\Omega(h_\sigma*f-g)(h_\sigma*\eta)dA.$$

By substituting the expression for $h_\sigma*\eta$ and exchanging variables, we obtain

$$\frac{\partial\mathcal{F}_\epsilon^I}{\partial\lambda}\bigg|_{\lambda=0}=\int_\Omega(h_\sigma*f-g)*h_\sigma(-x,-y)\eta(x,y)dA. \quad (21)$$

For the second part

$$\frac{\partial\mathcal{F}_\epsilon^{II}}{\partial\lambda}\bigg|_{\lambda=0}=2\beta\int_\Omega v^2(f_x\eta_x+f_y\eta_y)dA. \quad (22)$$

Integrating by parts yields

$$\frac{1}{2\beta}\frac{\partial\mathcal{F}_\epsilon^{II}}{\partial\lambda}\bigg|_{\lambda=0}=\int_\Omega\frac{\partial}{\partial x}(v^2\eta f_x)dA+\int_\Omega\frac{\partial}{\partial y}(v^2\eta f_y)dA-\int_\Omega\left[\frac{\partial}{\partial x}(v^2 f_x)+\frac{\partial}{\partial y}(v^2 f_y)\right]\eta dA.$$

By applying the divergence theorem to the vector field $v^2\eta\nabla f$, it is seen that the first two terms are equal to the closed contour integral

$$\int_{\partial\Omega}v^2\eta\nabla f\cdot dn \quad (23)$$

where n is the vector normal to the contour. Adopting the Neumann boundary condition

$$\frac{\partial f}{\partial n}=0\quad(x,y)\in\partial\Omega$$

integral (23) vanishes, hence (22) takes the form

$$\frac{\partial\mathcal{F}_\epsilon^{II}}{\partial\lambda}\bigg|_{\lambda=0}=-2\beta\int_\Omega\left[\frac{\partial}{\partial x}(v^2 f_x)+\frac{\partial}{\partial y}(v^2 f_y)\right]\eta dA. \quad (24)$$

Adding (21) and (24) and using the fundamental lemma of calculus of variations, we obtain (9)

$$\frac{\delta\mathcal{F}_\epsilon}{\delta f}=(h_\sigma*f-g)*h_\sigma(-x,-y)-2\beta\mathrm{Div}(v^2\nabla f)=0.$$

2) Variation With Respect to v: The variation of $\mathcal{F}_\epsilon$ with respect to v can be expressed as

$$\frac{\delta\mathcal{F}_\epsilon}{\delta v}=\frac{\partial}{\partial\lambda}\mathcal{F}_\epsilon(v+\lambda\psi)\bigg|_{\lambda=0}=\frac{\partial}{\partial\lambda}\left[\mathcal{F}_\epsilon^I+\mathcal{F}_\epsilon^{II}\right]\bigg|_{\lambda=0}=0$$

where

$$\mathcal{F}_\epsilon^I=\beta\int_\Omega(v+\lambda\psi)^2|\nabla f|^2 dA+\frac{\alpha}{4\epsilon}\int_\Omega(v+\lambda\psi-1)^2 dA$$

and

$$\mathcal{F}_\epsilon^{II}=\alpha\epsilon\int_\Omega\left[(v_x+\lambda\psi_x)^2+(v_y+\lambda\psi_y)^2\right]dA.$$

$$\frac{\partial\mathcal{F}_\epsilon^I}{\partial\lambda}\bigg|_{\lambda=0}=\int_\Omega\left[2\beta v|\nabla f|^2+\frac{\alpha}{2\epsilon}(v-1)\right]\psi dA \quad (25)$$

$$\frac{\partial\mathcal{F}_\epsilon^{II}}{\partial\lambda}\bigg|_{\lambda=0}=2\alpha\epsilon\int_\Omega[v_x\psi_x+v_y\psi_y]\,dA.$$

As with (22), we integrate by parts, apply the divergence theorem and adopt the Neumann boundary condition

$$\frac{\partial v}{\partial n}=0\quad(x,y)\in\partial\Omega$$

we obtain

$$\frac{\partial\mathcal{F}_\epsilon^{II}}{\partial\lambda}\bigg|_{\lambda=0}=-2\alpha\epsilon\int_\Omega(v_{xx}+v_{yy})\psi dA. \quad (26)$$

Adding (25) and (26), and using the fundamental lemma of calculus of variations, we arrive at (8)

$$\frac{\delta\mathcal{F}_\epsilon}{\delta v}=\left(2\beta|\nabla f|^2+\frac{\alpha}{2\epsilon}-2\alpha\epsilon\nabla^2\right)v=\frac{\alpha}{2\epsilon}$$

APPENDIX B

Theorem 1: The operator $A(v)$ defined as

$$A(v)=H_\sigma H_\sigma^*-2\beta\mathrm{Div}(v^2\nabla) \quad (27)$$

is self adjoint and positive definite.

Proof: Let $A(v) = A^I + A^{II}$, where

$$A^I u = H_\sigma H_\sigma^* u$$

and

$$A^{II} u = -2\beta \mathrm{Div}(v^2 \nabla u).$$

Let H be a convolution operator, i.e., $Hf(x) = h(x) * f(x)$ where $x \in \mathbb{R}^2$. Its adjoint operator H^* is defined by $\langle g, Hf\rangle = \langle H^* g, f\rangle$, where $\langle \cdot, \cdot \rangle$ denotes inner product. Here

$$\begin{aligned}\langle H^* g, f\rangle = \langle g, Hf\rangle &= \int_{\mathbb{R}^2} g \cdot (h * f) dx \\ &= \int_{\mathbb{R}^2} [h(-x) * g(x)] \cdot f(x) dx\end{aligned}$$

hence $H^* g(x) = h(-x) * g(x)$. Now

$$A^{I^*} u = h_\sigma(-x) * h_\sigma(x) * u = h_\sigma * h_\sigma(-x) * u = A^I u. \quad (28)$$

Thus A^I is a self adjoint operator.

Let $G(\xi)$ and $H(\xi)$ be the Fourier transforms of $g(x)$ and $h_\sigma(x)$, respectively, and let $\bar{G}(\xi), \bar{H}(\xi)$ be their complex conjugates. For a real function $g : \Omega \to \mathbb{R}, G(-\xi) = \bar{G}(\xi)$.

$$\begin{aligned}\langle g, A^I g\rangle &= \int_\Omega g(x)[h_\sigma(x) * h_\sigma(-x) * g(x)] dx \\ &= [G(\xi) * (H(\xi)\bar{H}(\xi) G(\xi))]_{\xi=0}.\end{aligned}$$

Substituting the convolution operator yields

$$\begin{aligned}\langle g, A^I g\rangle &= \left[\int_{\mathbb{R}^2} G(\xi - \xi')|H(\xi')|^2 G(\xi') d\xi'\right]_{\xi=0} \\ &= \int_{\mathbb{R}^2} G(-\xi') G(\xi') |H(\xi')|^2 d\xi' \\ &= \int_{\mathbb{R}^2} \bar{G}(\xi') G(\xi') |H(\xi')|^2 d\xi' \\ &= \int_{\mathbb{R}^2} |G(\xi')|^2 |H(\xi')|^2 d\xi' > 0\end{aligned}$$

for all functions g and kernels h_σ that are not identically zero, which proves that A^I is positive definite.

For the second part of the operator

$$\langle g, A^{II} f\rangle = -2\beta \int_\Omega g[\nabla \cdot (v^2 \nabla f)] dx.$$

Recall that for a scalar function g and a vector field ϕ

$$g \nabla \cdot \phi = \nabla \cdot (g\phi) - \nabla g \cdot \phi \quad (29)$$

thus

$$\langle g, A^{II} f\rangle = -2\beta \int_\Omega \nabla \cdot (g v^2 \nabla f) dx + 2\beta \int_\Omega \nabla g \cdot v^2 \nabla f dx.$$

Applying the divergence theorem

$$\langle g, A^{II} f\rangle = -2\beta \int_{\partial\Omega} \left(g v^2 \nabla f\right) \cdot dn + 2\beta \int_\Omega \nabla g \cdot v^2 \nabla f dx. \quad (30)$$

Using the Neumann boundary condition, the first term vanishes, hence

$$\begin{aligned}\langle g, A^{II} f\rangle &= 2\beta \int_\Omega \nabla g \cdot v^2 \nabla f dx \\ &= 2\beta \int_\Omega \nabla f \cdot v^2 \nabla g dx. \quad (31)\end{aligned}$$

Substituting (29) in (31) and using the divergence theorem, we obtain

$$\langle g, A^{II} f\rangle = 2\beta \int_{\partial\Omega} (g v^2 \nabla f) \cdot dn - 2\beta \int_\Omega f \nabla \cdot (v^2 \nabla g) dx.$$

Applying again the Neumann boundary condition, the first term vanishes and we observe that

$$\begin{aligned}\langle g, A^{II} f\rangle &= -2\beta \int_\Omega \nabla \cdot \left(v^2 \nabla g\right) f dx \\ &= \langle A^{II} g, f\rangle\end{aligned}$$

which proves that the operator A^{II} is self adjoint. We proceed to show that A^{II} is positive definite

$$\langle g, A_{II} g\rangle = -2\beta \int_\Omega g \nabla \cdot (v^2 \nabla g).$$

Applying (29) and using the divergence theorem yields

$$\langle g, A_{II} g\rangle = -2\beta \int_{\partial\Omega} (g v^2 \nabla g) \cdot dn + 2\beta \int_\Omega \nabla g \cdot (v^2 \nabla g) dx.$$

The first term vanishes due to the Neumann boundary condition, thus

$$\langle g, A_{II} g\rangle = 2\beta \int_\Omega v^2 |\nabla g|^2 dx > 0$$

we conclude that A^{II} is positive definite. Since both A^I and A^{II} are self adjoint and positive definite, their sum $A(v)$ is also self adjoint and positive definite. □

REFERENCES

[1] L. Ambrosio and V. M. Tortorelli, "Approximation of functionals depending on jumps by elliptic functionals via Γ-convergence," *Commun. Pure Appl. Math.*, vol. XLIII, pp. 999–1036, 1990.

[2] G. Aubert and P. Kornprobst, *Mathematical Problems in Image Processing*. New York: Springer, 2002.

[3] M. Banham and A. Katsaggelos, "Digital image restoration," *IEEE Signal Process. Mag.*, vol. 14, no. 2, pp. 24–41, Mar. 1997.

[4] L. Bar, N. Sochen, and N. Kiryati, "Variational pairing of image segmentation and blind restoration," in *Proc. ECCV'2004*. Prague, Czech Republic, 2004, pp. 166–177.

[5] A. Braides, *Approximation of Free-Discontinuity Problems*. Berlin, Germany: Springer, 1998, vol. 1694, pp. 47–51. Lecture Notes in Mathematics.

[6] A. S. Carasso, "Direct blind deconvolution," *SIAM J. Appl. Math.*, vol. 61, pp. 1980–2007, 2001.

[7] A. Chambolle, "Image segmentation by variational methods: Mumford and Shah functional, and the discrete approximation," *SIAM J. Appl. Math.*, vol. 55, pp. 827–863, 1995.

[8] T. Chan and C. Wong, "Total variation blind deconvolution," *IEEE Trans. Image Process.*, vol. 7, no. 3, pp. 370–375, Mar. 1998.

[9] P. Charbonnier, L. Blanc-Feraud, G. Aubert, and M. Barlaud, "Deterministic edge-preserving regularization in computed imaging," *IEEE Trans. Image Process.*, vol. 6, no. 2, pp. 298–311, Feb. 1997.

[10] D. Geman and C. Yang, "Nonlinear image recovery with half-quadratic regularization and FFT's," *IEEE Trans. Image Process.*, vol. 4, no. 7, pp. 932–946, Jul. 1995.
[11] J. Kim, A. Tsai, M. Cetin, and A. S. Willsky, "A curve evolution-based variational approach to simultaneous image restoration and segmentation," *Proc. IEEE ICIP*, vol. 1, pp. 109–112, 2002.
[12] D. Kundur and D. Hatzinakos, "Blind image deconvolution," *Signal Process. Mag.*, vol. 13, no. 6, pp. 43–64, Nov. 1996.
[13] D. Kundur and D. Hatzinakos, "Blind image deconvolution revisited," *Signal Process. Mag.*, vol. 13, pp. 61–63, Nov. 1996.
[14] D. Mumford and J. Shah, "Optimal approximations by piecewise smooth functions and associated variational problems," *Commun. Pure and Appl. Math.*, vol. 42, pp. 577–684, 1989.
[15] R. Nakagaki and A. Katsaggelos, "A VQ-based blind image restoration algorithm," *IEEE Trans. Image Process.*, vol. 12, no. 9, pp. 1044–1053, Sep. 2003.
[16] T. Richardson and S. Mitter, "Approximation, computation and distortion in the variational formulation," in *Geometery-Driven Diffusion in Computer Vision*, B. M. ter Harr Romeny, Ed. Boston, MA: Kluwer, 1994, pp. 169–190.
[17] L. Rudin, S. Osher, and E. Fatemi, "Non linear total variation based noise removal algorithms," *Physica D*, vol. 60, pp. 259–268, 1992.
[18] L. Rudin and S. Osher, "Total variation based image restoration with free local constraints," in *Proc. IEEE ICIP*, vol. 1, Austin, TX, 1994, pp. 31–35.
[19] C. Samson, L. Blanc-Féraud, G. Aubert, and J. Zerubia, "Multiphase Evolution and Variational Image Classification,", Tech. Rep. 3662, Apr. 1999. INRIA Sophia Antipolis.
[20] M. Sonka, V. Hlavac, and R. Boyle, *Image Processing, Analysis and Machine Vision*. Boston, MA: PWS-Kent, 1999.
[21] F. Sroubek and J. Flusser, "Multichannel blind iterative image restoration," *IEEE Trans. Image Process.*, vol. 12, no. 9, pp. 1094–1106, Sep. 2003.
[22] A. Tikhonov and V. Arsenin, *Solutions of Ill-Posed Problems*. New York: Wiley, 1977.
[23] L. A. Vese and T. F. Chan, "A multiphase level set framework for image segmentation using the Mumford and Shah model," *Int. J. Comput. Vis.*, vol. 50, pp. 271–293, 2002.
[24] C. Vogel and M. Oman, "Fast, robust total variation-based reconstruction of noisy, blurred images," *IEEE Trans. Image Process.*, vol. 7, no. 6, pp. 813–824, Jun. 1998.
[25] E. W. Weisstein *et al.*. Minimal residual method. *MathWorld—A Wolfram Web Resource* [Online]. Available: http://mathworld.wolfram.com/MinimalResidualMethod.html
[26] Y. You and M. Kaveh, "A regularization approach to joint blur identification and image restoration," *IEEE Trans. Image Process.*, vol. 5, no. 3, pp. 416–428, Mar. 1996.

Leah Bar received the B.Sc. degree in physics from Bar-Ilan University, Ramat Gan, Israel, in 1990 and the M.Sc. degree in bio-medical engineering in 1994 from Tel-Aviv University, Tel-Aviv, Israel, where she is currently pursuing the Ph.D. degree in the School of Electrical Engineering.

Nir Sochen received the B.Sc. degree in physics in 1986 and the M.Sc. degree in theoretical physics in 1988 from the University of Tel-Aviv, Tel-Aviv, Israel, and the Ph.D. degree in theoretical physics in 1992 from the Université de Paris-Sud, Paris, France, while conducting his research in the Service de Physique Théorique at the Centre d'Etude Nucleaire, Saclay, France.

He was with the Ecole Normale Superieure, Paris, on a Haute Etude Scientifique fellowship, and then a three-year National Science Foundation fellowship in the Physics Department, University of California at Berkeley. He spent one year in the Physics Department, University of Tel-Aviv, and two years in the Faculty of Electrical Engineering, Technion-Israel Institute of Technology. Currently, he is a Senior Lecturer in the Department of Applied Mathematics, Tel-Aviv University. His early research were in the fields of quantum field theories and integrable models related to high-energy physics and string theory. More recently, he has focused on computer vision and image processing, particularly the applications of differential geometry and statistical physics in image processing and computational vision.

Nahum Kiryati (M'94–SM'95) received the B.Sc. degree in electrical engineering and the Post-B.A. degree in Humanities from the University of Tel-Aviv, Tel-Aviv, Israel, in 1980 and 1986, respectively. He received the M.Sc. degree in electrical engineering in 1988 and the D.Sc. degree in 1991, both from The Technion, Israel Institute of Technology, Haifa, Israel.

He was with the Image Science Laboratory, ETH-Zurich, Zurich, Switzerland, and with the Department of Electrical Engineering, The Technion. He is now with the School of Electrical Engineering, Tel-Aviv University. His research interests are in image analysis and computer vision.